

Graphene-incorporated hyaluronic acid-based hydrogel as a controlled Senexin A delivery system

Panita Maturavongsadit¹, Weiwei Wu², Jingyu Fan¹, Igor B. Roninson³, Taixing Cui^{2,*}, Qian Wang^{1,*}

Key Words:

controlled drug delivery; graphene oxide; hyaluronic acid-based hydrogel; Senexin A

From the Contents

Introduction	152
Methods	153
Results	155
Discussion	158

ABSTRACT

Perivascular delivery of therapeutic agents against established aetiologies for occlusive vascular remodelling has great therapeutic potential for vein graft failure. However, none of the perivascular drug delivery systems tested experimentally have been translated into clinical practice. In this study, we established a novel strategy to locally and sustainably deliver the cyclin-dependent kinase 8/19 inhibitor Senexin A (SenA), an emerging drug candidate to treat occlusive vascular disease, using graphene oxide-hybridised hyaluronic acid-based hydrogels. We demonstrated an approach to accommodate SenA in hyaluronic acid-based hydrogels through utilising graphene oxide nanosheets allowing for non-covalent interaction with SenA. The resulting hydrogels produced sustained delivery of SenA over 21 days with tunable release kinetics. *In vitro* assays also demonstrated that the hydrogels were biocompatible. This novel graphene oxide-incorporated hyaluronic acid hydrogel offers an optimistic outlook as a perivascular drug delivery system for treating occlusive vascular diseases, such as vein graft failure.

*Corresponding authors:

Taixing Cui,
Taixing.Cui@uscmed.sc.edu;
Qian Wang,
wang263@mailbox.sc.edu.

<http://doi.org/10.12336/biomatertransl.2022.02.007>

How to cite this article:

Maturavongsadit, P.; Wu, W.; Fan, J.; Roninson, I. B.; Cui, T.; Wang, Q. Graphene-incorporated hyaluronic acid-based hydrogel as a controlled Senexin A delivery system. *Biomater Transl.* 2022, 3(2), 152-161.

Introduction

Perivascular delivery of therapeutic agents against established aetiologies for occlusive vascular remodelling has great therapeutic potential for vein graft failure.¹⁻⁶ This mode of application has clear advantages: systemic side effects are avoided, clinically-established drugs can be used, and the application would be clinically feasible. Nevertheless, none of the perivascular drug delivery systems tested experimentally have been translated into clinical practice, at least partly due to the lack of a perivascular drug delivery system for vein grafts. Given that transplanted vein grafts are usually not restricted by surrounding tissues but instead are freely suspended, therapeutic drug delivery cannot be achieved if the matrix carrying drugs cannot firmly adhere to the adventitia of vein grafts with minimal impact on vein graft mechanics. Indeed, it is a challenge to create such a drug delivery system.

Hyaluronic acid (HA)-based hydrogels have been widely used for numerous drug delivery applications due to their biocompatibility, biodegradability, and tunable physicochemical properties.⁷⁻⁹ HA-based hydrogels provide high porosity and permeability, allowing for drug loading and release via a diffusion process. However, the uses of HA hydrogels in drug delivery applications remain limited by low drug payloads, particularly for hydrophobic drugs and rapid release kinetics.^{10, 11} Therefore, modifying the microstructure of HA-based hydrogels,¹² and/or incorporating micro-¹³ and nanoparticles,¹⁴⁻¹⁶ could be adopted to control drug release from HA hydrogels. Graphene oxide nanosheet (GO) has been demonstrated to have potential uses in various biomedical applications, such as drug delivery systems,^{17, 18} tissue-engineered scaffolds,^{19, 20} and biosensors.^{21, 22} GO is a derivative of graphene containing hydroxyl,



Controlled drug delivery by graphene/HA-based hydrogels

carbonyl, carboxyl and epoxide functional groups on the surfaces. It provides a very highly-specific surface area, excellent aqueous solubility, biocompatibility, and multi-functionalities. Due to the presence of π electrons delocalised on its surface, GO provides the ability to interact with hydrophobic drugs or molecules containing aromatic species through π - π stacking and electrostatic or hydrophobic interactions.²³⁻²⁸

In this study, we developed GO-hybridised HA-based hydrogels that (1) provided sustained release of Senexin A (SenA), a selective inhibitor of cyclin-dependent kinase 8/19,²⁹ an emerging drug candidate for occlusive vascular disease (our unpublished data) *in vitro* at a therapeutic concentration of 3–30 μ M for 3 weeks or longer, and (2) were biodegradable and nontoxic. GO served as a nanoparticle for improving SenA payloads and controlling the SenA release rate. The HA-based hydrogel was used as a biodegradable macroscale polymeric scaffold to retain and localise the SenA-loaded GO nanocarriers in a vascular microenvironment. SenA was first loaded into GO (GO-SenA) via strong π - π and electrostatic interactions. Next, GO-SenA was *in-situ* encapsulated into HA-based hydrogel to form GO-SenA-loaded HA hydrogels (Figure 1). The physicochemical properties, release kinetics, biocompatibility, and efficacy of GO-SenA-loaded HA hydrogels were then evaluated in *in vitro* models.

Methods

Preparation of graphene oxide nanosheets

GO were synthesised following the method described in previous reports.^{30, 31} Briefly, dried graphite flakes (1 g, Graphene Supermarket[®]; Graphene Laboratories Inc., Ronkonkoma, NY, USA) were dispersed in 50 mL of

concentrated sulphuric acid (95% w/w) while stirring in an ice bath. Potassium permanganate (3 g, > 99%, Sigma-Aldrich, St. Louis, MO, USA) was subsequently added into the suspension at room temperature (25°C), stirred for 25 minutes, and sonicated for 5 minutes, repeating this stirring-sonication process for 12 cycles. Distilled water (200 mL) was then added to quench the reaction. The suspension was further sonicated for 2 hours to obtain GO. The resulting GO was washed using the modified Hummers' method.^{30,31} Briefly, hydrogen peroxide (20 mL, 30% v/v, Merck-Millipore, Darmstadt, Germany) was added into the GO suspension while stirring until no more gas was released. The GO precipitates were washed thrice in hydrochloric acid (1 M) using centrifugation at $10,060 \times g$ for 30 minutes followed by distilled water thrice. The final GO precipitates were dried in an oven at 40°C for 3 days.

Preparation of drug-loaded graphene oxide

SenA (Senex Biotechnology, Columbia, SC, USA) and GO were added to 3 mL phosphate-buffered saline (PBS; pH 7.4) and sonicated for 1 hour prior to stirring for 20 hours at room temperature protected from light. The product (GO-SenA) was collected by repeated centrifugation at $15,300 \times g$ for 5 minutes and washing with PBS until the supernatant became colourless. The resulting GO-SenA was freeze-dried. The amount of unbound SenA was determined by measuring the absorbance at 323 nm using an ultraviolet-visible (UV-VIS) spectrometer (Nanodrop 2000; Thermo Scientific[™], Wilmington, DE, USA) relative to a calibration curve recorded under identical conditions. The SenA-loading efficiency was calculated as follows: SenA-loading efficiency (%) = $(W_{\text{freeSenA}} - W_{\text{feedSenA}}) / W_{\text{feedSenA}} \times 100$.

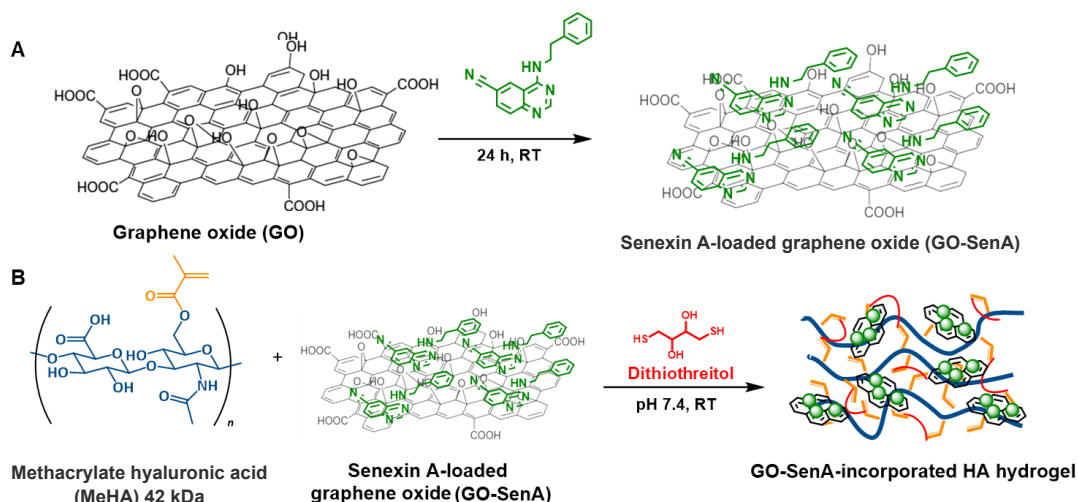


Figure 1. (A) Schematic illustrating the synthesis of Senexin A-loaded graphene (GO-SenA) hyaluronic acid (HA)-based hydrogels via Michael addition reaction. (B) GO-SenA was first prepared and then *in-situ* encapsulated to form a GO-SenA-incorporated HA-based hydrogel. RT: room temperature.

1 Department of Chemistry and Biochemistry, University of South Carolina, Columbia, SC, USA; 2 Department of Cell Biology and Anatomy School of Medicine Columbia, University of South Carolina, Columbia, SC, USA; 3 Department of Drug Discovery & Biomedical Sciences, College of Pharmacy, University of South Carolina, Columbia, SC, USA

Physicochemical properties of graphene oxide and drug-loaded graphene oxide

GO and GO-SenA were characterised by UV-VIS spectrophotometry, Fourier transform infrared spectroscopy (FTIR) (Spectrum-GX, PerkinElmer, Waltham, MA, USA), and scanning electron microscopy (Zeiss Ultraplus Thermal Field Emission, Carl Zeiss Microscopy GmbH, Jena, Germany) using previous protocols.^{32, 33}

Formation of drug-loaded graphene hyaluronic acid hydrogels

Prior to the formation of the GO-SenA-loaded HA hydrogels, methacrylate-modified HA polymer at approximately 50% modification (50 DM MeHA) was first synthesised following our previously-reported methods.^{32, 33} The GO-SenA was dispersed in medium (PBS or Dulbecco's modified Eagle's medium (DMEM)) at 0.1% (w/v) by sonication for 2 hours. Then 50 DM MeHA was added into the GO-SenA suspension at a concentration of 3% (w/v). After MeHA was completely dissolved in the GO-SenA mixture, 0.5 M dithiothreitol (DTT) was added to form the GO-SenA-loaded HA hydrogel. For comparative purposes, SenA-loaded HA hydrogels were prepared using the same procedures and compositions of MeHA, DTT, and SenA as GO-SenA-loaded HA hydrogels, but without GO. GO-loaded HA hydrogels were also prepared using the same procedures and compositions of MeHA, DTT, and GO as GO-SenA-loaded HA hydrogels, but without SenA loading.

Gelation time

GO-SenA-loaded HA hydrogels were prepared following a previously-described method using PBS as the medium. Gelation time was measured by the vial tilting method.³⁴ When the sample showed no flow within 20 seconds, it was considered to be completely formed hydrogel.

Mechanical properties

The complex modulus of the GO-SenA-loaded HA hydrogels was measured using a DHR-3 rheometer (TA Instrument, New Castle, DE, USA) with 12-mm diameter parallel-plate geometry and a temperature-controlled Peltier plate. The hydrogels were prepared as previously described using DMEM as the medium. After gelling, the samples were subjected to frequency sweeps (0.1–10 rad/s) at 1% strain amplitude. The geometry gap was controlled by axial force at 0.2 N in each run.

In vitro drug release study

Hydrogel constructs were incubated in a 96-well plate with 100 μ L of release DMEM at 37°C with gentle shaking. At each time-point, an aliquot was removed for analysis and replaced with fresh DMEM over a time-course of 21 days. The amount of released SenA at each time-point was quantified in the aliquots by UV-VIS spectrometry (at 323 nm) relative to a standard curve of SenA recorded under identical conditions. The release kinetics of SenA were analysed using different kinetic models for controlled drug delivery systems, including zero order, first order, Higuchi, and Korsmeyer-Peppas model equations.³⁵

Zero-order release model: $Q_t = K_0 t$

First-order release model: $\ln(100 - Q_t) = \ln 100 - K_1 t$

Higuchi release model: $Q_t = K_h t^{1/2}$

Korsmeyer-Peppas model: $Q_t/Q_e = K t^n$

where Q_t is the percentage of drug released at time t ; Q_t/Q_e is the fraction of the SenA released at time t ; K_0 , K_1 , K_h and K represent the zero-order release kinetic constant, the first-order release kinetic constant, the Higuchi release kinetic constant and the Korsmeyer-Peppas kinetic constant incorporating structural and geometric characteristics of the hydrogel, respectively; and n is the release exponent, indicative of the mechanism of drug release. Namely, the case of $n \leq 0.45$ corresponds to a Fickian diffusion (diffusion-controlled drug release; the rate of release is independent of the drug concentration in the hydrogels.), $0.45 < n < 0.89$ to a non-Fickian transport, $n = 0.89$ to Case II transport (erosion-controlled drug release), and $n > 0.89$ to super case II transport mechanism. When determining the n exponent, only the portions of the release curve where the absolute cumulative amounts of drug released at time $t \leq 60\%$ were used.

Vascular smooth muscle cell isolation and culture

Aortic arches and roots (1.5 cm in length) from male 8-week-old C57BL/6J mice (25.0 ± 1.4 g; Jackson Laboratory, Bar Harbor, ME, USA) were collected in accordance with the guidelines for animal experimentation by the Institutional Animal Care and Use Committee, School of Medicine, University of South Carolina (animal protocol approval No. 2446-101412-041019; approval date: April 10, 2019). The mice were euthanized by overdose of carbon dioxide. All experiments were designed and reported according to the Animal Research: Reporting of *In Vivo* Experiments (ARRIVE) guidelines.³⁶ The adventitia was separated from the aorta under a microscope. The aortic vessels were cut into small pieces and enzymatically digested for 70 minutes at 37°C with 50% w/v collagenase type 2 (Worthington Biochemical Corporation, Lakewood, NJ, USA) in 10% foetal bovine serum supplemented DMEM (High Glucose, Gibco™, Carlsbad, CA, USA). Subsequently, the digestion was quenched by adding ice-cold 10% foetal bovine serum-supplemented DMEM. Vascular smooth muscle cells (VSMCs) were filtered and pelleted at $300 \times g$ for 8 minutes. VSMCs were cultured and incubated in completed medium (DMEM high glucose containing 20% foetal bovine serum, penicillin (100 U/mL) and streptomycin (100 mg/mL) for 6–7 days. The medium was changed every 2 days. The purity of cultured VSMCs was verified by immunohistochemical staining of smooth muscle alpha actin. The cultured aortic VSMCs between passages 3–10 in which ~99% of cells were positive for smooth muscle alpha actin were used in this study.

In vitro cytocompatibility

VSMCs were analysed by CellTiter-Blue (CTB) cell viability assay (Promega, Madison, WI, USA) after 24 hours of culture in a 96-well plate with GO-SenA-loaded HA or GO-loaded HA hydrogels (prepared following the method described above) or with cells alone as the positive control. Cell culture

medium was replaced with 200 μL of prewarmed medium containing 15% CTB and incubated for 2 hours at 37°C with 5% CO_2 . Medium containing CTB without cells was used as the negative control. The medium containing the metabolite of CTB was measured for fluorescence intensity at 560/590 nm using a SpectraMax M2 Multi-Mode microplate reader (Molecular Devices, Sunnyvale, CA, USA).

Statistical analysis

All data are expressed as mean \pm standard deviation (SD). The differences between groups were analysed by one-way analysis of variance followed by Dunnett's multiple comparison test using GraphPad Prism 5.0 (GraphPad Software, San Diego, CA, USA, www.graphpad.com). A value of $P < 0.05$ was considered to be statistically.

Results

Preparation of drug-loaded graphene oxide and drug-loaded graphene hyaluronic acid hydrogels

The goal of this development was to sustain delivery of SenA *in vitro* in the therapeutic concentration range of 3–30 μM for 3 weeks or longer. GOs were utilised to directly interact with SenA via π - π stacking and electrostatic or hydrophobic interactions. In this study, GOs were synthesised from graphene flakes and provided a size range of 200 nm–3.5 μm based on scanning electron microscopic imaging (Figure 2A). The presence of hydroxyl, carbonyl and carboxyl functionalities were observed using FTIR. The spectra of GO showed (1) a broad characteristic peak at 3600–3200 cm^{-1} corresponding

to the stretching vibration of the OH group, (2) strong peaks between 1800–1600 cm^{-1} corresponding to the stretching vibration of the C=O carbonyl group, and (3) peaks at 1170, 1090 and 1050 cm^{-1} corresponding to the C–O stretching vibrations (Figure 2B).^{31, 37} Additionally, the synthesised GO was highly water-soluble, which was considerably different from the graphene flakes prior to modification (Figure 2C, and D). These results confirmed that the GOs were successfully synthesised from graphene flakes.

After confirming the physiochemical properties of the synthesised GO, GO-SenA was generated by stirring SenA and GO in PBS for 24 hours at room temperature (Figure 1A). The successful attachment of SenA to GO was confirmed by FTIR and UV-VIS spectrometry (Figure 3A, and B). Compared with SenA and GO, the FTIR spectrum of GO-SenA at 1:3 loading ratio of GO:SenA showed peaks at 3400, 3100–3010, 2260 cm^{-1} (corresponding to stretching bands of amine N–H, alkenyl C–H, and nitrile C \equiv N, respectively, of SenA) and at 1600 and 900–600 cm^{-1} (corresponding to the bending band and wagging bands of amine N–H from SenA), in addition to the weak characteristic peaks belonging to GO. It should be noted that the observed characteristic peaks from SenA were dominant in the FTIR of GO-SNX due to high SenA loading to GO. Additionally, the UV-VIS spectrum of GO-SenA showed pronounced absorbance at both 230, and 323 nm, due to the absorbance of GO and SNX respectively (Figure 3B). By varying the ratios of GO:SenA, SenA was successfully attached to GO with almost 100% loading efficiency as confirmed by UV-VIS spectrometry (Figure 3C).

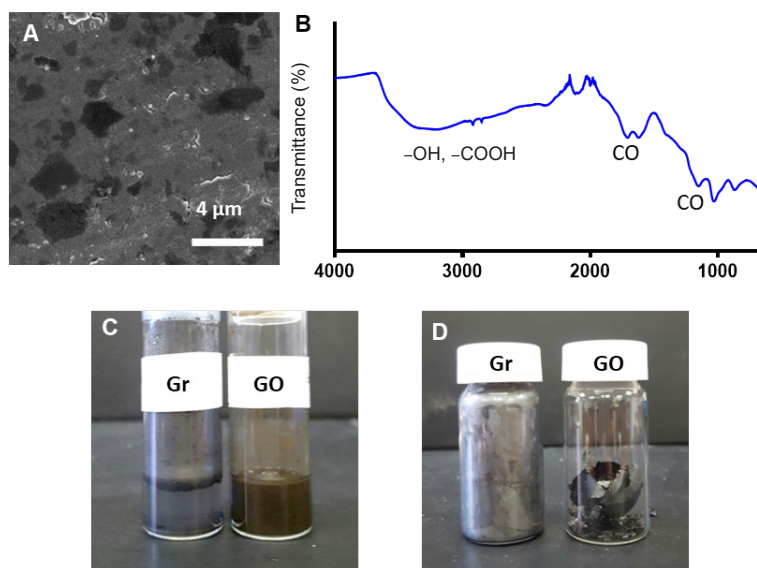


Figure 2. Characterisation of the synthesised GO. (A) Scanning electron microscopic image of the synthesised GO after sonication for 1 hour. Scale bar: 4 μm . (B) Fourier transform infrared spectroscopic spectrum of the synthesised GO. (C) Physical appearances of graphene and the synthesised GO dispersed in phosphate-buffered saline. (D) Physical appearances of graphene and the synthesised GO after drying. GO: graphene oxide nanosheet; Gr: graphene flakes.

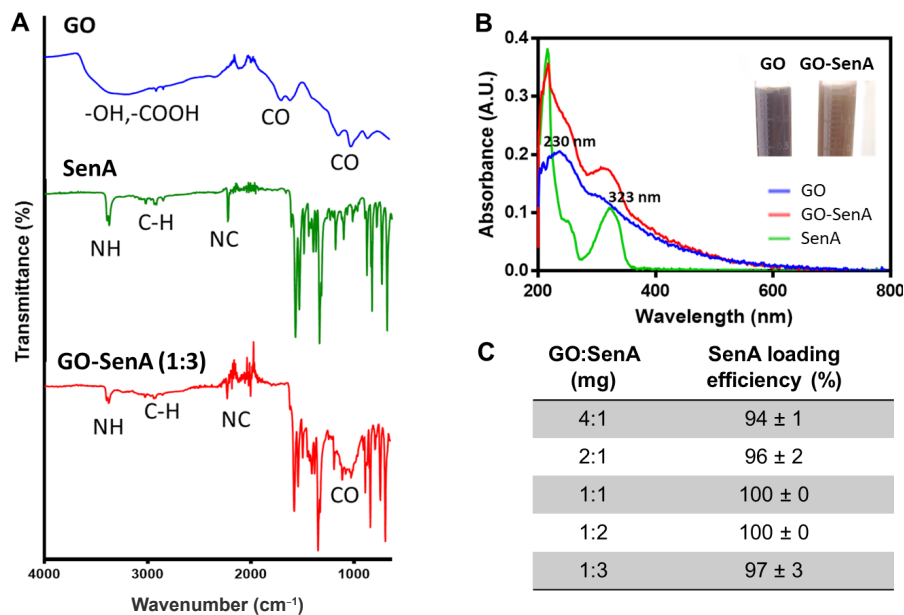


Figure 3. Preparation and characterisation of GO-SenA. (A) Fourier transform infrared spectra of GO, SenA, and GO-SenA. (B) Ultraviolet-visible spectra of GO, SenA, and GO-SenA. (C) Loading efficiency of SenA onto GO at different weight ratios ($n = 3$). A.U.: absorbance unit; GO: graphene oxide nanosheet; GO-SenA: Senexin A-loaded graphene oxide nanosheet; SenA: Senexin A.

The GO-SenA-loaded HA hydrogel was formed by mixing 3% (w/v) of MeHA polymer with 0.1% (w/v) of GO-SenA in PBS, followed by adding DTT as a crosslinker (**Figure 1**). Without the addition of DTT, the mixture of GO-SenA and HA was highly viscous due to the electrostatic interaction (H-bonding). Nevertheless, this interaction was not strong enough to create a hydrogel. The Michael reaction between the thiol group of DTT and the methacrylate group of HA occurred after adding DTT, resulting in hydrogel formation.

Gelation time and mechanical properties of Senexin A-loaded graphene hyaluronic acid hydrogels

The gelation time and mechanical properties of hydrogels are some of the essential criteria in the development of a perivascular drug delivery system. Due to the restricted time for which a decellularised vessel can be exposed to the environment, the coating application of the hydrogel onto a decellularised vessel should be completed within approximately 20 minutes. Therefore, the gelation of the

hydrogel should occur within 20 minutes, and the hydrogel must be highly flexible and attachable to the decellularised vessel. The gelation times of HA-based hydrogels were first screened using varying concentrations of HA and DTT (**Additional Table 1**). Based on the results of this screening process, 3% HA was selected as the master formulation and GO-SenA-loaded HA formulations with varying DTT and GO-SenA concentrations were investigated. The results showed that increasing the concentration of DTT promoted the gelation process. However, DTT also affected the gelation process in different ways depending on the concentration of GO-SenA. Specifically, at lower concentrations of DTT (2 and 4 $\mu\text{L}/100 \mu\text{L}$), using higher GO-SenA concentration (0.3% (w/v)) prolonged the gel formation time of GO-SenA-loaded HA hydrogels. In contrast, at a high concentration of DTT (6 $\mu\text{L}/100 \mu\text{L}$), using a high GO-SenA concentration led to fast crosslinking (8–10 minutes) of a rigid graphene scaffold (**Table 1**, and **Additional Figure 1A**).

Table 1. Gelation times of different GO-SenA loaded HA hydrogels which were determined by the tilting method

Formulation	MeHA (%w/v)	0.5 M DTT-Crosslinker ($\mu\text{L}/100 \mu\text{L}$)	GO-SenA (1:3) (%w/v)	Gelation time (min)
1	3	2	0.1	35–48
2	3	2	0.3	50–96
3	3	4	0.1	30–35
4	3	4	0.3	40–50
5	3	6	0.1	8–12
6	3	6	0.3	6–10

Note: DTT: dithiothreitol; GO: graphene oxide nanosheet; HA: hyaluronic acid; MeHA: methacrylate modified hyaluronic acid; SenA: Senexin A.

Controlled drug delivery by graphene/HA-based hydrogels

The complex modulus of the optimised GO-SenA-loaded HA hydrogels was further characterised after gelling and subsequently incubating for 3 days. The complex modulus of the hydrogels after gelling and 3-day incubation were approximately 35 and 100 Pa, respectively, and they were highly flexible and soft (Figure 4, and Additional Figure 1B–E). The hydrogels were also easily applied *in situ* to the decellularised vessels by the drop-coating technique (Additional Figure 2). The hydrogels were firmly attached to the vessel scaffolds and were stable after storage for 1 day in PBS. Based on these results, the hydrogel formulation containing low DTT and GO-SenA concentrations was selected as the master recipe for subsequent studies.

In vitro drug release of Senexin A-loaded graphene hyaluronic acid hydrogels

In vitro release studies of SenA from GO-SNX-loaded HA hydrogels compared to SenA-loaded HA hydrogels were conducted to investigate the effect of GO in the hydrogel system on SenA release. The result showed that the 2-hour burst release of SenA from the GO-SenA-loaded HA was considerably slower than that from SenA-loaded HA hydrogels (Figure 5A). The release rate of SenA from the GO-SenA HA systems remained constant at $\sim 100 \mu\text{M}/\text{d}$, while the release rate of SenA from the SenA-loaded HA hydrogels was considerably faster ($\sim 250 \mu\text{M}/\text{d}$) and subsequently slowed down at 5 days (Figure 5B, and C).

In vitro release studies of SenA from GO-SenA-loaded HA hydrogels with different loading ratios of GO:SenA were further investigated to modulate the release rate of SenA within the therapeutic window, ranging from 3–30 μM . It was found that increasing the ratio of GO:SenA considerably slowed the release rate of SenA (Figure 5D). The 4:1 loading

ratio of GO:SenA was found to be optimal to sustain the release of SenA at $\sim 30 \mu\text{M}/\text{d}$ for ~ 21 days (Figure 5E). A slight dose dumping was observed on day 22 due to the degradation of HA polymers (Figure 5F).

The release kinetics of SenA from the GO-SenA-loaded HA hydrogels were further analysed using different kinetic models, including zero order, first order, and Higuchi model equations.³⁵ As shown in Additional Figure 3 and Additional Table 2, the release of SenA from GO in HA-based hydrogels best fitted the first-order kinetics model ($R^2 \sim 0.95\text{--}0.98$), where the drug release rate depended on its concentration in the hydrogel system. The Korsmeyer-Peppas kinetic model was further used to understand the release mechanism of SenA from the hydrogel system.³⁸ The mechanism of drug release from the Korsmeyer-Peppas model is indicated by the release exponent (n). The higher ratio of GO:SenA incorporated into hydrogels, the higher the n values observed from fitting data to the Korsmeyer-Peppas model. The n values from fitting data of the SenA release from GO-SenA HA (4:1), GO-SenA HA (1:1), and GO-SenA HA (1:3) hydrogels were 0.5445, 0.3678, and 0.2764, respectively. Based on these n values, the release of SenA from GO-SenA HA (4:1) hydrogels matched to the combination of diffusion and erosion-controlled rate release mechanism while the release of SenA from GO-SenA HA (1:1) and (1:3) hydrogels fitted to the diffusion-controlled rate release mechanism only.

In vitro cytocompatibility of Senexin A-loaded graphene hyaluronic acid hydrogels

Cytotoxicity is one of the properties of biomaterials which have important effects for drug delivery. The CTB assay results showed no cytotoxicity in VSMCs when cultured with GO-SenA-loaded HA hydrogels for 24 hours (Figure 6).

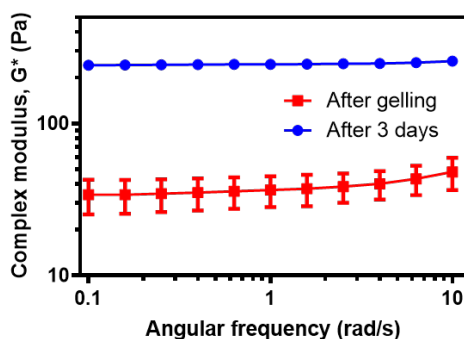


Figure 4. Mechanical properties of the optimised GO-SenA-loaded HA hydrogels immediately after gelation, and 3 days after gelation. The values are expressed as mean \pm SD ($n = 3$). GO: graphene oxide nanosheet; HA: hyaluronic acid; SenA: Senexin A.

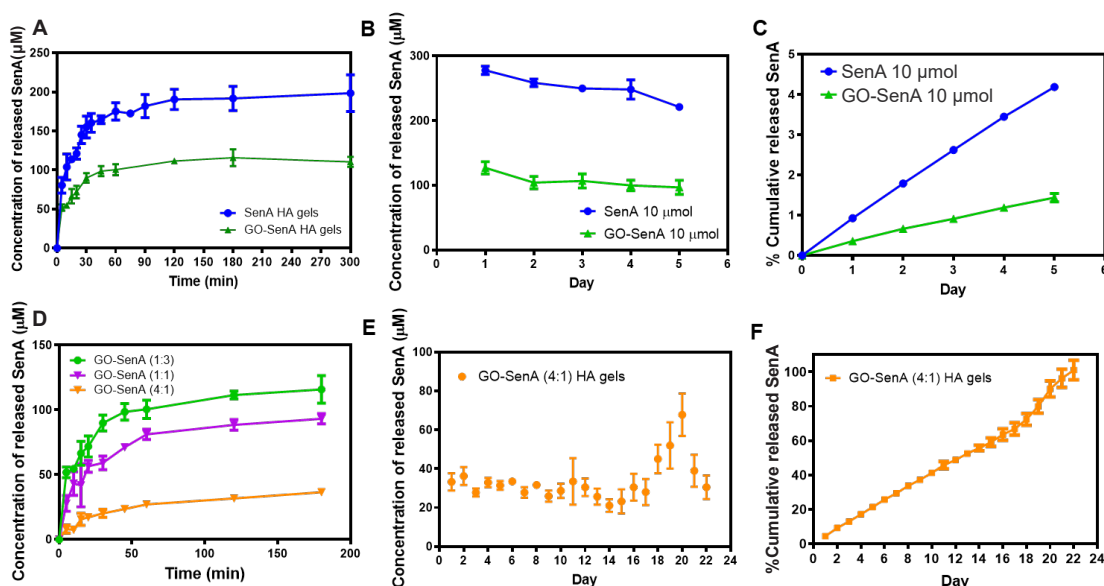


Figure 5. *In vitro* SenA release profiles of GO-SenA-loaded HA hydrogels. (A) *In vitro* SenA release profiles of GO-SenA HA hydrogels compared to SenA loaded HA hydrogels over the first 5 hours of incubation in phosphate-buffered saline at 37°C. (B) *In vitro* SenA release profiles of GO-SenA HA hydrogels and SenA loaded HA hydrogels over 5 days in phosphate-buffered saline at 37°C. (C) *In vitro* cumulative release profile of SenA from GO-SenA HA and SenA-loaded HA hydrogels calculated from B. SenA concentration loaded into both GO-SenA HA and SenA-loaded HA hydrogels were equal at 10 µmol per hydrogel. (D) *In vitro* SenA release profiles of GO-SenA HA hydrogels using different loading ratios of GO:SenA (1:3, 1:1, and 4:1). (E) *In vitro* SenA release profiles of GO-SenA HA hydrogels using 4:1 loading ratio of GO:SenA. (F) The cumulative release profile of SenA from GO-SenA HA hydrogels shown in E. All values are expressed as mean ± SD ($n = 3$). GO: graphene oxide nanosheet; HA: hyaluronic acid; SenA: Senexin A.

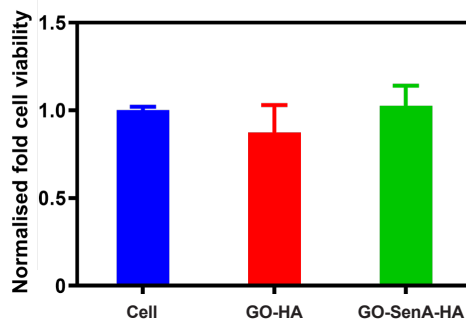


Figure 6. *In vitro* cytocompatibility of GO-SenA-loaded HA hydrogels. (A) Cell viability of vascular smooth muscle cells after culturing in primary medium with GO-HA hydrogels or GO-SenA-loaded HA hydrogels or without any hydrogel for 24 hours using CellTiter-Blue assay. The data were normalised to the cell viability intensity of cell alone (positive control). The values expressed are mean ± SD ($n = 3$) from two repeated experiments. GO: graphene oxide nanosheet; HA: hyaluronic acid; SenA: Senexin A.

Discussion

Herein, we report on a biodegradable GO-incorporated HA-based hydrogel that is adhesive to the adventitia of vessel grafts and can accommodate and deliver SenA within a therapeutic concentration range (3–30 µM) (our unpublished data). The biodegradable GO-incorporated HA-based hydrogels were prepared through a two-step process: (a) SenA loading onto GO surfaces, and (b) *in-situ* forming GO-SenA-loaded HA hydrogels by Michael reaction of thiol from DTT and from

the methacrylate group on HA polymers. Our study showed that SenA was successfully loaded onto GO surfaces at various ratios such as 4:1, 2:1, 1:1, 1:2 and 1:3 of GO:SenA with very high loading efficiency of over 90%. This high-efficiency loading can be ascribed to the strong hydrogen-bond and π - π stacking interactions between SenA and GO.³⁹⁻⁴³ In addition, we found that GO-SenA-loaded HA hydrogels 3-day post-incubation showed higher complex modulus than the gels after immediate gelation. This is likely ascribed to the physical

Controlled drug delivery by graphene/HA-based hydrogels

interactions (i.e., hydrogen bonding and electrostatic forces) of GO and HA occurring post-incubation, leading to higher complex modulus of the hydrogel. There was a limit on the amount of GO-SenA and DTT that could incorporate into this HA-based hydrogel system. Using too high concentrations of DTT and GO-SenA led to fast crosslinking of graphene scaffold instead of forming GO-SenA-incorporated HA-based hydrogels. This is because DTT can serve as the reducing agent to reduce GO to a graphene scaffold.

The release kinetics of SenA from GO-SenA-loaded HA hydrogels were highly controllable, and sustained compared to SenA released from HA hydrogels. This is due to the strong hydrogen-bond and π - π stacking interactions between SenA and GO at pH 7.4 that controlled the release of SenA from the networks.³⁹⁻⁴¹ Mathematical kinetic modelling revealed that the drug release mechanism from GO-SenA-loaded HA hydrogels was mainly driven by diffusion and erosion depending on the ratio of GO:SenA. Solutes transported from HA-based material systems could be driven by diffusion and/or degradation of HA under physiological conditions.^{44, 45} More importantly, due to the interaction between the SenA and GO components, the SenA release rate could be further controlled by GO in the HA-based systems. The fast release of SenA (dose dumping) was observed between days 18 and 20 prior to the completion of SenA release. It is likely attributed to the complete degradation of HA network.

The *in vitro* assays using VSMCs demonstrated that GO-SenA-loaded HA hydrogels were biocompatible and degradable,³² supporting their potential use *in vivo*. However, the *in vivo* long-term safety of the materials should be considered in future studies, particularly with regard to GO. It has been reported that single-layer GO sheets were internalised and sequestered in cytoplasmic, membrane-bound vacuoles by human lung epithelial or fibroblast cells and induced toxicity at doses above 20 $\mu\text{g}/\text{mL}$ after 24 hours.⁴⁶ GO, and pristine graphene were both recognised by macrophages, leading to cell activation and secretion of pro-inflammatory cytokines.⁴⁷⁻⁵⁰ These effects were dependent on the geometry of the graphene used. Larger flakes ($\sim 2 \mu\text{m}$) provoked a significantly increased secretion of inflammatory cytokines by macrophages *in vitro* compared to the smaller flakes ($\sim 350 \text{ nm}$).⁵¹ Consequently, further optimisation of the GO lateral sizes for the long-term safety of GO-SenA-loaded HA hydrogels should be our next development step. Additionally, the pharmacokinetics of the release of SenA from GO-SenA-loaded HA hydrogels will need to be investigated, and the release kinetics may need to be further optimised for *in vivo* models of vein graft transplantation.

Although many polymeric materials have been investigated as perivascular drug delivery systems over the past several decades, such as poly(lactic-co-glycolic) acid,⁵²⁻⁵⁴ poloxamer,⁵⁵ polyvinyl acetate,⁵⁶ and polyethylene glycol^{57, 58} materials, no efficient perivascular treatment is yet available. Thus far, the only product to successfully undergo phase III clinical trial is SirogenTM, a sirolimus-eluting collagen wrap for use on patients on haemodialysis. Developing an effective perivascular

drug delivery system is highly challenging due to its complex requirements. Specifically, the perivascular drug delivery systems must provide appropriate mechanical properties that ensure system localisation, prolonged retention, and adequate vascular constriction. More importantly, the release kinetics of pharmacological agents should match the development of the pathology. Given that the physicochemical properties of these GO-HA-based hydrogels are easily and highly tunable through chemical functionalisation of either HA^{32, 33} or GO, we envision that GO-HA-based hydrogels could be a promising perivascular drug delivery platform for the treatment of vascular diseases.

In summary, this study demonstrated that GO-SenA-loaded HA hydrogels provided sustained delivery of SenA and exhibited good efficacy with high biocompatibility *in vitro*. Considering that longer implantation times will be required for the applications, the *in vitro* degradation time, mechanical properties, and cytotoxicity of GO-SenA-loaded HA hydrogels at longer incubation times should be investigated in the future study. Additionally, several aspects may need to be considered prior to moving forward this technology into clinical practice, including the *in vivo* pharmacokinetics and efficacy in inhibition of occlusive vascular remodelling and short-term and long-term safety of the biomaterial. The versatility of this technology also makes it attractive as a perivascular drug delivery platform for the treatment of vascular diseases.

Author contributions

Conceptualisation, methodology, project administration and funding acquisition: TC, QW; study design and data generation: PM, FJ, WW; data curation, investigation, and validation: PM, TC and QW; manuscript review and editing: PM, FJ, TC, QW. All authors approved the final version of this manuscript.

Financial support

The work was supported by United States NIH under the award Nos. R01 GM136877 (to QW, JF), R43 HL137525 (to TC), R21 EB022131 (to TC), P20 GM1090991 (to TC), and R01 HL160541 (to TC).

Acknowledgement

None.

Conflicts of interest statement

The authors declare no competing financial interest.

Editor note: Qian Wang is an Editorial Board Member of *Biomaterials Translational*, but was blocked from reviewing or making decisions on the manuscript. The article was subject to the journal's standard procedures, with peer review handled independently of the Editorial Board member and his research group.

Open access statement

This is an open access journal, and articles are distributed under the terms of the Creative Commons Attribution-NonCommercial-ShareAlike 4.0 License, which allows others to remix, tweak, and build upon the work non-commercially, as long as appropriate credit is given and the new creations are licensed under the identical terms.

Additional files

Additional Figure 1: The formation and physical appearances of rigid graphene scaffold.

Additional Figure 2: The attachment of Senexin A-loaded graphene HA hydrogels to the decellularised scaffolds in phosphate-buffered saline immediately after gelling (A) and 1 day later (B).

Additional Figure 3: Fitting of the data for SenA release from the SenA-loaded HA hydrogels (SenA-HA) and GO-SenA HA hydrogels having different loading ratios of GO:SenA (1:3, 1:1, and 4:1) into phosphate-buffered saline (pH 7.4) to the zero order (A) and first order kinetics (B).

Additional Table 1: Screening gelation times of HA-based hydrogels without SenA and GO incorporation.

Additional Table 2: Correlation coefficient (R^2), rate constant (K), and release exponent (n) values obtained by fitting the data of the release of SenA from different hydrogel formulations into phosphate-buffered saline at pH 7.4.

1. Sanders, W. G.; Hoglebe, P. C.; Grainger, D. W.; Cheung, A. K.; Terry, C. M. A biodegradable perivascular wrap for controlled, local and directed drug delivery. *J Control Release*. **2012**, *161*, 81-89.
2. Katare, R.; Riu, F.; Rowlinson, J.; Lewis, A.; Holden, R.; Meloni, M.; Reni, C.; Wallrapp, C.; Emanuelli, C.; Madeddu, P. Perivascular delivery of encapsulated mesenchymal stem cells improves postischemic angiogenesis via paracrine activation of VEGF-A. *Arterioscler Thromb Vasc Biol*. **2013**, *33*, 1872-1880.
3. Masaki, T.; Rathi, R.; Zentner, G.; Leypoldt, J. K.; Mohammad, S. F.; Burns, G. L.; Li, L.; Zhuplatov, S.; Chirananthavat, T.; Kim, S. J.; Kern, S.; Holman, J.; Kim, S. W.; Cheung, A. K. Inhibition of neointimal hyperplasia in vascular grafts by sustained perivascular delivery of paclitaxel. *Kidney Int*. **2004**, *66*, 2061-2069.
4. Mylonaki, I.; Allémann, É.; Saucy, F.; Haefliger, J. A.; Delie, F.; Jordan, O. Perivascular medical devices and drug delivery systems: Making the right choices. *Biomaterials*. **2017**, *128*, 56-68.
5. Wu, B.; Werlin, E. C.; Chen, M.; Mottola, G.; Chatterjee, A.; Lance, K. D.; Bernards, D. A.; Sansbury, B. E.; Spite, M.; Desai, T. A.; Conte, M. S. Perivascular delivery of resolvin D1 inhibits neointimal hyperplasia in a rabbit vein graft model. *J Vasc Surg*. **2018**, *68*:188S-200S.e4.
6. Lee, J.; Jang, E. H.; Kim, J. H.; Park, S.; Kang, Y.; Park, S.; Lee, K.; Kim, J. H.; Youn, Y. N.; Ryu, W. Highly flexible and porous silk fibroin microneedle wraps for perivascular drug delivery. *J Control Release*. **2021**, *340*, 125-135.
7. Uman, S.; Dhand, A.; Burdick, J. A. Recent advances in shear-thinning and self-healing hydrogels for biomedical applications. *J Appl Polym Sci*. **2020**, *137*, 48668.
8. Dovedytis, M.; Liu, Z. J.; Bartlett, S. Hyaluronic acid and its biomedical applications: A review. *Engineered Regen*. **2020**, *1*, 102-113.
9. Tiwari, S.; Bahadur, P. Modified hyaluronic acid based materials for biomedical applications. *Int J Biol Macromol*. **2019**, *121*, 556-571.
10. Trombino, S.; Servidio, C.; Curcio, F.; Cassano, R. Strategies for hyaluronic acid-based hydrogel design in drug delivery. *Pharmaceutics*. **2019**, *11*, 407.
11. Ghasemiyeh, P.; Mohammadi-Samani, S. Hydrogels as drug delivery systems; pros and cons. *Trends Pharm Sci*. **2019**, *5*, 7-24.
12. Fu, S.; Xiao, X.; Dong, H.; Zhang, Z.; Zhang, X.; Zhong, Z.; Zhuo, R. An injectable hyaluronic acid/PEG hydrogel produced via copper-free click chemistry for drug delivery. *J Control Release*. **2017**, *259*, e123-e124.
13. França, C. G.; Plaza, T.; Naveas, N.; Andrade Santana, M. H.; Manso-Silván, M.; Recio, G.; Hernandez-Montelongo, J. Nanoporous silicon microparticles embedded into oxidized hyaluronic acid/adipic acid dihydrazide hydrogel for enhanced controlled drug delivery. *Microporous Mesoporous Mater*. **2021**, *310*, 110634.
14. Merino, S.; Martín, C.; Kostarelos, K.; Prato, M.; Vázquez, E. Nanocomposite hydrogels: 3D polymer-nanoparticle synergies for on-demand drug delivery. *ACS Nano*. **2015**, *9*, 4686-4697.
15. Yegappan, R.; Selvaprithiviraj, V.; Mohandas, A.; Jayakumar, R. Nano polydopamine crosslinked thiol-functionalized hyaluronic acid hydrogel for angiogenic drug delivery. *Colloids Surf B Biointerfaces*. **2019**, *177*, 41-49.
16. Min, Q.; Liu, J.; Zhang, Y.; Yang, B.; Wan, Y.; Wu, J. Dual network hydrogels incorporated with bone morphogenic protein-7-loaded hyaluronic acid complex nanoparticles for inducing chondrogenic differentiation of synovium-derived mesenchymal stem cells. *Pharmaceutics*. **2020**, *12*, 613.
17. Asadi, H.; Ghaee, A.; Nourmohammadi, J.; Mashak, A. Electrospun zein/graphene oxide nanosheet composite nanofibers with controlled drug release as antibacterial wound dressing. *Int J Polymeric Mater Polymeric Biomater*. **2020**, *69*, 173-185.
18. Ghawanmeh, A. A.; Ali, G. A. M.; Algarni, H.; Sarkar, S. M.; Chong, K. F. Graphene oxide-based hydrogels as a nanocarrier for anticancer drug delivery. *Nano Res*. **2019**, *12*, 973-990.
19. Kolanthai, E.; Sindu, P. A.; Khajuria, D. K.; Veerla, S. C.; Kuppuswamy, D.; Catalani, L. H.; Mahapatra, D. R. Graphene oxide-A tool for the preparation of chemically crosslinking free alginate-chitosan-collagen scaffolds for bone tissue engineering. *ACS Appl Mater Interfaces*. **2018**, *10*, 12441-12452.
20. Choe, G.; Oh, S.; Seok, J. M.; Park, S. A.; Lee, J. Y. Graphene oxide/alginate composites as novel bioinks for three-dimensional mesenchymal stem cell printing and bone regeneration applications. *Nanoscale*. **2019**, *11*, 23275-23285.
21. Yildiz, G.; Bolton-Warberg, M.; Awaja, F. Graphene and graphene oxide for bio-sensing: General properties and the effects of graphene ripples. *Acta Biomater*. **2021**, *131*, 62-79.
22. Gosai, A.; Khondakar, K. R.; Ma, X.; Ali, M. A. Application of functionalized graphene oxide based biosensors for health monitoring: simple graphene derivatives to 3D printed platforms. *Biosensors (Basel)*. **2021**, *11*, 384.
23. Geim, A. K.; Novoselov, K. S. The rise of graphene. *Nat Mater*. **2007**, *6*, 183-191.
24. Kim, K. S.; Zhao, Y.; Jang, H.; Lee, S. Y.; Kim, J. M.; Kim, K. S.; Ahn, J. H.; Kim, P.; Choi, J. Y.; Hong, B. H. Large-scale pattern growth of graphene films for stretchable transparent electrodes. *Nature*. **2009**, *457*, 706-710.
25. Service, R. F. Materials science. Carbon sheets an atom thick give rise to graphene dreams. *Science*. **2009**, *324*, 875-877.
26. Zhou, X.; Liu, Z. A scalable, solution-phase processing route to graphene oxide and graphene ultralarge sheets. *Chem Commun (Camb)*. **2010**, *46*, 2611-2613.
27. Pandey, H.; Parashar, V.; Parashar, R.; Prakash, R.; Ramteke, P. W.; Pandey, A. C. Controlled drug release characteristics and enhanced antibacterial effect of graphene nanosheets containing gentamicin sulfate. *Nanoscale*. **2011**, *3*, 4104-4108.
28. Miao, W.; Shim, G.; Lee, S.; Lee, S.; Choe, Y. S.; Oh, Y. K. Safety and tumor tissue accumulation of pegylated graphene oxide nanosheets for co-delivery of anticancer drug and photosensitizer. *Biomaterials*. **2013**, *34*, 3402-3410.
29. Porter, D. C.; Farmaki, E.; Altiglia, S.; Schools, G. P.; West, D. K.; Chen, M.; Chang, B. D.; Puzyrev, A. T.; Lim, C. U.; Rokow-Kittell, R.; Friedhoff, L. T.; Papavassiliou, A. G.; Kalurupalle, S.; Hurteau, G.; Shi, J.; Baran, P. S.; Gyroffly, B.; Wentland, M. P.; Broude, E. V.; Kiaris, H.; Roninson, I. B. Cyclin-dependent kinase 8 mediates chemotherapy-induced tumor-promoting paracrine activities. *Proc Natl Acad Sci U S A*. **2012**, *109*, 13799-13804.
30. Yu, H.; Zhang, B.; Bulin, C.; Li, R.; Xing, R. High-efficient synthesis of graphene oxide based on improved hummers method. *Sci Rep*. **2016**, *6*, 36143.
31. Marcano, D. C.; Kosynkin, D. V.; Berlin, J. M.; Sinitskii, A.; Sun, Z.; Slesarev, A.; Alemany, L. B.; Lu, W.; Tour, J. M. Improved synthesis of

Controlled drug delivery by graphene/HA-based hydrogels

- graphene oxide. *ACS Nano*. **2010**, *4*, 4806-4814.
32. Maturavongsadit, P.; Bi, X.; Metavarayuth, K.; Luckanagul, J. A.; Wang, Q. Influence of cross-linkers on the in vitro chondrogenesis of mesenchymal stem cells in hyaluronic acid hydrogels. *ACS Appl Mater Interfaces*. **2017**, *9*, 3318-3329.
 33. Maturavongsadit, P.; Luckanagul, J. A.; Metavarayuth, K.; Zhao, X.; Chen, L.; Lin, Y.; Wang, Q. Promotion of in vitro chondrogenesis of mesenchymal stem cells using in situ hyaluronic hydrogel functionalized with rod-like viral nanoparticles. *Biomacromolecules*. **2016**, *17*, 1930-1938.
 34. Hiemstra, C.; Zhou, W.; Zhong, Z.; Wouters, M.; Feijen, J. Rapidly in situ forming biodegradable robust hydrogels by combining stereocomplexation and photopolymerization. *J Am Chem Soc*. **2007**, *129*, 9918-9926.
 35. Dash, S.; Murthy, P. N.; Nath, L.; Chowdhury, P. Kinetic modeling on drug release from controlled drug delivery systems. *Acta Pol Pharm*. **2010**, *67*, 217-223.
 36. Kilkenny, C.; Browne, W. J.; Cuthill, I. C.; Emerson, M.; Altman, D. G. Improving bioscience research reporting: the ARRIVE guidelines for reporting animal research. *PLoS Biol*. **2010**, *8*, e1000412.
 37. Gurunathan, S.; Han, J. W.; Kim, E. S.; Park, J. H.; Kim, J. H. Reduction of graphene oxide by resveratrol: a novel and simple biological method for the synthesis of an effective anticancer nanotherapeutic molecule. *Int J Nanomedicine*. **2015**, *10*, 2951-2969.
 38. Korsmeyer, R. W.; Gurny, R.; Doelker, E.; Buri, P.; Peppas, N. A. Mechanisms of solute release from porous hydrophilic polymers. *Int J Pharm*. **1983**, *15*, 25-35.
 39. Wang, H.; Gu, W.; Xiao, N.; Ye, L.; Xu, Q. Chlorotoxin-conjugated graphene oxide for targeted delivery of an anticancer drug. *Int J Nanomedicine*. **2014**, *9*, 1433-1442.
 40. Depan, D.; Shah, J.; Misra, R. D. K. Controlled release of drug from folate-decorated and graphene mediated drug delivery system: Synthesis, loading efficiency, and drug release response. *Mater Sci Eng C*. **2011**, *31*, 1305-1312.
 41. Lv, Y.; Tao, L.; Annie Bligh, S. W.; Yang, H.; Pan, Q.; Zhu, L. Targeted delivery and controlled release of doxorubicin into cancer cells using a multifunctional graphene oxide. *Mater Sci Eng C Mater Biol Appl*. **2016**, *59*, 652-660.
 42. Yang, D.; Gao, S.; Fang, Y.; Lin, X.; Jin, X.; Wang, X.; Ke, L.; Shi, K. The π - π stacking-guided supramolecular self-assembly of nanomedicine for effective delivery of antineoplastic therapies. *Nanomedicine (Lond)*. **2018**, *13*, 3159-3177.
 43. Song, J.; Cui, N.; Sun, S.; Lu, X.; Wang, Y.; Shi, H.; Lee, E. S.; Jiang, H. B. Controllability of graphene oxide doxorubicin loading capacity based on density functional theory. *Nanomaterials (Basel)*. **2022**, *12*, 479.
 44. Bonacucina, G.; Cespi, M.; Palmieri, G. F. Evaluation of dissolution kinetics of hydrophilic polymers by use of acoustic spectroscopy. *Int J Pharm*. **2009**, *377*, 153-158.
 45. Siepman, J.; Göpferich, A. Mathematical modeling of bioerodible, polymeric drug delivery systems. *Adv Drug Deliv Rev*. **2001**, *48*, 229-247.
 46. Sanchez, V. C.; Jachak, A.; Hurt, R. H.; Kane, A. B. Biological interactions of graphene-family nanomaterials: an interdisciplinary review. *Chem Res Toxicol*. **2012**, *25*, 15-34.
 47. Girish, C. M.; Sasidharan, A.; Gowd, G. S.; Nair, S.; Koyakutty, M. Confocal Raman imaging study showing macrophage mediated biodegradation of graphene in vivo. *Adv Healthc Mater*. **2013**, *2*, 1489-1500.
 48. Chen, G. Y.; Yang, H. J.; Lu, C. H.; Chao, Y. C.; Hwang, S. M.; Chen, C. L.; Lo, K. W.; Sung, L. Y.; Luo, W. Y.; Tuan, H. Y.; Hu, Y. C. Simultaneous induction of autophagy and toll-like receptor signaling pathways by graphene oxide. *Biomaterials*. **2012**, *33*, 6559-6569.
 49. Zhou, H.; Zhao, K.; Li, W.; Yang, N.; Liu, Y.; Chen, C.; Wei, T. The interactions between pristine graphene and macrophages and the production of cytokines/chemokines via TLR- and NF- κ B-related signaling pathways. *Biomaterials*. **2012**, *33*, 6933-6942.
 50. Russier, J.; Treossi, E.; Scarsi, A.; Perrozzi, F.; Dumortier, H.; Ottaviano, L.; Meneghetti, M.; Palermo, V.; Bianco, A. Evidencing the mask effect of graphene oxide: a comparative study on primary human and murine phagocytic cells. *Nanoscale*. **2013**, *5*, 11234-11247.
 51. Yue, H.; Wei, W.; Yue, Z.; Wang, B.; Luo, N.; Gao, Y.; Ma, D.; Ma, G.; Su, Z. The role of the lateral dimension of graphene oxide in the regulation of cellular responses. *Biomaterials*. **2012**, *33*, 4013-4021.
 52. Aviles-Olmos, I.; Dickson, J.; Kefalopoulou, Z.; Djamshidian, A.; Kahan, J.; Ell, P.; Whitton, P.; Wyse, R.; Isaacs, T.; Lees, A.; Limousin, P.; Foltynie, T. Motor and cognitive advantages persist 12 months after exenatide exposure in Parkinson's disease. *J Parkinsons Dis*. **2014**, *4*, 337-344.
 53. Zhu, W.; Masaki, T.; Bae, Y. H.; Rathi, R.; Cheung, A. K.; Kern, S. E. Development of a sustained-release system for perivascular delivery of dipyridamole. *J Biomed Mater Res B Appl Biomater*. **2006**, *77*, 135-143.
 54. Edelman, E. R.; Nathan, A.; Katada, M.; Gates, J.; Karnovsky, M. J. Perivascular graft heparin delivery using biodegradable polymer wraps. *Biomaterials*. **2000**, *21*, 2279-2286.
 55. Schachner, T.; Zou, Y.; Oberhuber, A.; Tzankov, A.; Mairinger, T.; Laufer, G.; Bonatti, J. O. Local application of rapamycin inhibits neointimal hyperplasia in experimental vein grafts. *Ann Thorac Surg*. **2004**, *77*, 1580-1585.
 56. Okada, T.; Bark, D. H.; Mayberg, M. R. Localized release of perivascular heparin inhibits intimal proliferation after endothelial injury without systemic anticoagulation. *Neurosurgery*. **1989**, *25*, 892-898.
 57. Lipke, E. A.; West, J. L. Localized delivery of nitric oxide from hydrogels inhibits neointima formation in a rat carotid balloon injury model. *Acta Biomater*. **2005**, *1*, 597-606.
 58. Masters, K. S.; Lipke, E. A.; Rice, E. E.; Liel, M. S.; Myler, H. A.; Zygourakis, C.; Tulis, D. A.; West, J. L. Nitric oxide-generating hydrogels inhibit neointima formation. *J Biomater Sci Polym Ed*. **2005**, *16*, 659-672.

Received: April 11, 2022

Revised: May 16, 2022

Accepted: May 30, 2022

Available online: June 28, 2022